Eur. Phys. J. Appl. Phys. **98**, 34 (2023)

https://doi.org/10.1051/epjap/2023220293

THE EUROPEAN PHYSICAL JOURNAL APPLIED PHYSICS

Regular Article

In situ TEM study of crystals growth in amorphous Ti-Zr-Ni films at electron beam irradiation

Aleksandr Bagmut*, Ivan Bagmut, and Aleksandr Devizenko

National Technical University "Kharkiv Polytechnic Institute", NTU "KhPI" 2, Kyrpychova str., 61002, Kharkiv, Ukraine

Received: 22 November 2022 / Received in final form: 17 March 2023 / Accepted: 12 April 2023

Abstract. Using the methods of in situ transmission electron microscopy (TEM) with video recording of the phase transformations the structure and kinetics of crystal growth in amorphous films of $Ti_{41}Zr_{41}Ni_{18}$ were studied. The films were obtained by magnetron sputtering of a Ti-Zr-Ni target with deposition on substrates at $T = 30$ °C. The amorphous (X-ray amorphous) state of the film was retained up to a temperature of 650 °C, above which a polymorphous transformation took place with the formation of crystals with the fcc structure. Video frame analysis shows that the nucleation and growth of flat crystals with fcc structure take place at electron beam irradiation. The speed of movement of the crystallization front did not depend on the time at a constant intensity of the electron beam. A linear dependence on time for the radius of the crystal and a quadratic one for the fraction of the crystalline phase are performed. The dimensionless parameter of the relative length of crystallization was about three thousand.

1 Introduction

Practical and scientific interest in Ti-Zr-Ni films and coatings is due to their property to dissolve a large amount of hydrogen (up to two hydrogen atoms for each metallic atom) [1–3]. Moreover, it is known, that these systems present a quasicrystalline phase for the different compositions of Ti, Ni and Zr [3–7]. Quasicrystallinity, suggesting a large number of tetrahedral sites, as well as the affinity of Ti and Zr atoms for hydrogen, makes these compound potentially useful materials for storing hydrogen for fuel cells and batteries [3].

The deposition of both atomic and vapor-plasma flows of Ti, Ni, and Zr on a substrate at room temperature, leads to the formation of amorphous films. Films of Ti-Zr-Ni, deposited by thermal evaporation [8], laser [3,4] and magnetron sputtering [6,7,9] on the substrate at the room temperature, are amorphous (or X-ray-amorphous). Rising of the substrate temperature T_S higher than 160 °C initiates the formation of crystalline (or quasi-crystalline) films. The finely dispersed $Ti_{41.5}Ni_{17}Zr_{41}$ icosahedral phase with a grain size of 2–10 nm was formed on sapphire substrates in the temperature range $T_S = 160$–350 °C during laser sputtering of Ti–Ni–Zr ingots [3]. With magnetron sputtering of Ti-Zr-Ni alloy target amorphous and fcc-(Ti, Zr)2Ni phase predominate in the Ti-Zr-Ni films when the substrate temperatures are in the range of 100–400 °C and 500–600 °C respectively [9].

Annealing of X-ray-amorphous films of composition $Ti_{53}Zr_{30}Ni_{18}$ and $Ti_{41}Zr_{38.3}Ni_{20.7}$ at temperatures above 673 K initiated the formation of a quasicrystalline phases with the characteristic parameters $a_0 = 0.517$ and 0.5205 nm respectively [7]. A single study with transmission electron microscopy of the structure of the initial X-ray-amorphous and final quasicrystalline state in the $Ti_{41}Zr_{38.3}Ni_{20.7}$ (at.%) film after thermal annealing at 500 °C for 59 h is given in [6]. Despite the above data, the structure and kinetics of the transformation of the amorphous (X-ray-amorphous) – crystalline (quasicrystalline) state at annealing of the Ti-Zr-Ni films has not been studied enough.

This work aims at carrying out of the study of the structure and kinetics of crystal growth during electron beam irradiation of amorphous $Ti_{41}Zr_{41}Ni_{18}$ films. TEM with in situ video registration of structural evolution offers the possibility to do it. Frame by frame analysis of the video allowed real-time measurement of the size and growth rate of crystals, as well as the degree of crystallinity of the film under study.

2 Experimental

Amorphous films with 20 nm thickness were prepared on an Al_2O_3 and KCl single-crystal substrates at 30 °C by the method of direct-current magnetron sputtering of a target with the composition $Ti_{41}Zr_{41}Ni_{18}$ (at.%). Sputtering was carried out in purified argon at the pressure of 2×10^{-1} Pa. The chemical composition of the grown films corresponded to the composition of the target, that was confirmed by the method of X-ray fluorescence analysis [10]. Description of the preparation procedure of amorphous films is given in [6,7]. After deposition and depressurization of the chamber the substrate of KCl together with the deposited film (the film is on the top of the substrate) were placed in distilled

* e-mail: agbagmut@gmail.com

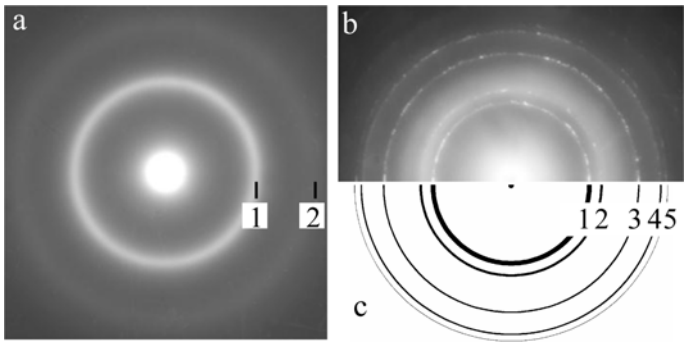

Fig. 1. Electron diffraction patterns of $Ti_{41}Zr_{41}Ni_{18}$ film in the initial state (a) and after partial electron beam crystallization (b), as well as its theoretical scheme (c).

water. The crystal was partially dissolved and the film floated freely on the surface of the water. With the help of tweezers, the film was caught by an object grid (mesh 270 in the form of a disk with a diameter of 3 mm), which was previously placed in water under the film. Excess water was carefully removed with filter paper at the point of contact between the grid and tweezers.

Morphology and structure of the crystals were studied by electron diffraction and in situ TEM with electron microscopes EM-100L and PEM-100-01 at the accelerating voltage of 100 kV. Crystallisation was initiated with thermal annealing of the film on substrate of Al_2O_3 and by the influence of the electron beam inside the electron microscope. This made it possible to register the structural transformations in situ. Besides using an electron beam focused to a diameter of 2–5 μm at beam current of 20 μA, one can perform the beam density j varying from 6.37 A/mm^2 (dose rate $\sim 39.8 \times 10^4$ e$^-$/Å$^2\cdot$s) to 1.02 A/mm^2 (dose rate $\sim 6.4 \times 10^4$ e$^-$/Å$^2\cdot$s) for different heating conditions. The crystallization rate increased monotonically with increasing of j at any desired region of the film.

The crystallization process was recorded with a Canon Power Shot G15 camera at the frame rate of 30 s^{-1}. So, the error in time $\Delta t = 30^{-1}$ s. According to [11] using a specialized computer program, we measured the total area, occupied by the crystals at the electron microscope image of the analyzed space of the film. The content of the crystalline fraction x in the video frame we defined as the ratio

$$x = \frac{S(t)}{S(t_f)}, \tag{1}$$

where $S(t)$ is the area occupied by the crystalline phase in the frame at an arbitrary time moment t. $S(t_f)$ is the area occupied by the crystalline phase in the frame at the end of filming (at time moment t_f). The crystal radius $R(t)$ at a time t was determined according to the relation

$$R(t) = \sqrt{\frac{S_k(t)}{\pi}}, \tag{2}$$

where $S_k(t)$ is the area of the crystal image at the time t. If only one crystal grows in the field of observation, then $S(t) \equiv S_k(t)$.

3 Results and discussion

Figure 1a shows the electron diffraction pattern from the free-standing film of $Ti_{41}Zr_{41}Ni_{18}$ immediately after its separation from the substrate of KCl. It consists of two diffraction halos. The first halo is intense, while the second one is much weaker in the intensity and very diffuse. These electron diffraction data indicate on the amorphous nature of this film.

Figure 1b shows the electron diffraction pattern of the same $Ti_{41}Zr_{41}Ni_{18}$ film after exposure to an electron beam in microscope column of individual sections of the grid with amorphous film. Electron beam heating of the film did not lead to the complete disappearance of the primary halo, but in addition to them one can see a system of point reflections located in a ring. Second diffraction ring, corresponding to interplanar distance $d = 0.251$ nm, appear near the diffraction halo number 1, as well as fourth diffraction ring, corresponding to interplanar distance $d = 0.152$ nm, appear near the diffraction halo number 2. Analysis shows that all rings correspond to disoriented crystals, which belong to the face centered cubic (fcc) phase.

The experimental electron diffraction pattern (Fig. 1b) is superimposed with the theoretical electron diffraction pattern for the polycrystalline film with the fcc structure (Fig. 1c). The radii of the circles of the theoretical electron diffraction pattern ρ satisfy the relation:

$$\rho = G\sqrt{h^2 + k^2 + l^2}, \tag{3}$$

where G is the scaling factor and h, k, l are the Miller indices of the crystal planes. Reflections for which h, k and l are numbers with different parity are forbidden. The corresponding circles are not shown in the theoretical electron diffraction pattern. Changing the scale factor G, it is possible to achieve complete coincidence of the rings of the experimental electron diffraction pattern with the circles of

Table 1. The results of the decoding of the electron diffraction pattern at Figure 1.

Amorphous state		Crystal state			
Diffraction halo number	d (nm)	Diffraction ring number	hkl	d (nm)	a_0 (nm)
1	0.25	1	111	0.289	0.502 ± 0.005
		2	200	0.251	
		3	220	0.177	
2	0.15	4	311	0.152	
		5	222	0.145	

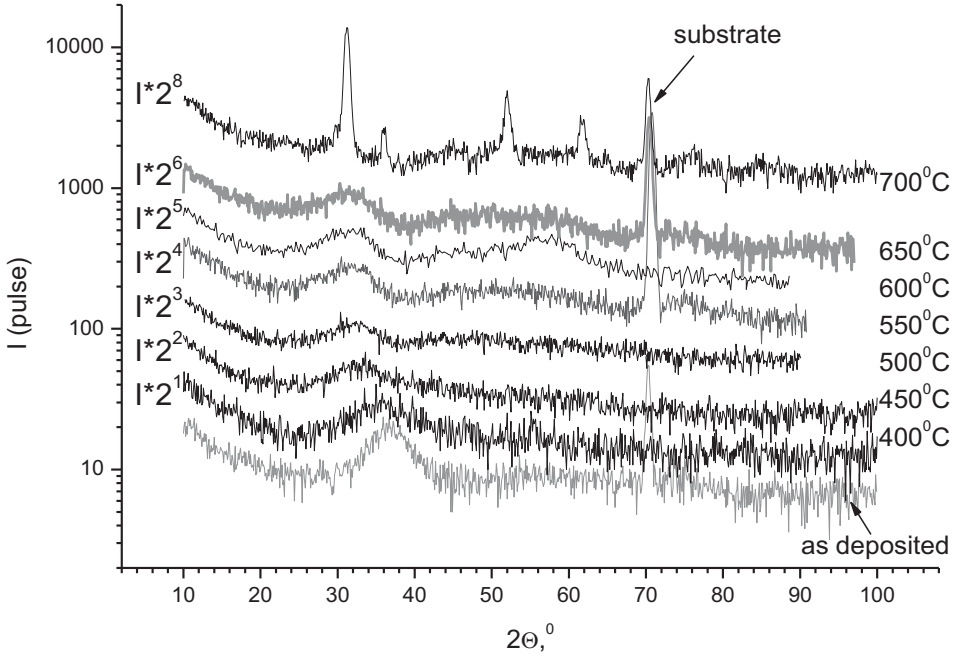

Fig. 2. X-ray diffraction patterns (Cu-Kα radiation) for a $Ti_{41}Zr_{41}Ni_{18}$ coating of 20 nm thick on an Al_2O_3 single-crystal substrate in as deposited state and after 1 hour of annealing at each temperature in vacuum ($\sim 7 \cdot 10^{-4}$ Pa).

the theoretical one, when they are superimposed. Therefore, the reflections numbered 1, 2, 3, etc. are can be assigned with indices h, k, l of the fcc lattice.

The result of the decoding of the electron diffraction pattern in Figure 1 is summarized in Table 1. According to Table 1, it follows that the fcc $Ti_{41}Zr_{41}Ni_{18}$ phase with the cubic lattice parameter $a_0 = 0.502 \pm 0.005$ nm is formed upon electron beam irradiation of amorphous film.

The electron diffraction data correspond to the X-ray phase analysis data. Figure 2 shows diffraction patterns (Cu-Kα radiation, 2Θ scan mode, sample is fixed at the grazing angle of $\Theta = 1.4°$) for a $Ti_{41}Zr_{41}Ni_{18}$ coating of 20 nm thick on an Al_2O_3 single-crystal substrate in the initial state and after annealing.

At as deposited state the coating is X-ray amorphous. The diffraction pattern shows one wide halo centered near the angle $2\Theta = 37^0$. The diffraction maximum near the angle $2\Theta = 71^0$ is due to diffraction from the sapphire substrate after the passage of the X-ray beam through the coating. As the annealing temperature increases, the halo shifts toward smaller angles. The X-ray amorphous state of the coating is preserved up to a temperature of 650 °C. At a temperature of 700 °C, the coating crystallizes. Two diffraction lines appear near the halo $2\Theta = 32^o$ and $2\Theta = 36^o$, as well as two lines near $2\Theta = 52^o$ and $2\Theta = 62^o$. According to estimation from Scherrer formula [12] the coherent scattering region (CSR) size in the direction perpendicular to the film for the most intense lines near the angles $2\Theta = 31°$, $2\Theta = 52°$ and $2\Theta = 62°$ is ~ 22 nm. This is comparable to a film thickness of 20 nm. That is, the crystalline phase extends over the entire thickness of the film.

The result of the decoding of the X-ray diffraction pattern (Fig. 2) of coating annealed at the temperature of 700 °C is summarized in Table 2. According to it follows, that the fcc $Ti_{41}Zr_{41}Ni_{18}$ phase with the cubic lattice parameter $a_0 = 0.497 \pm 0.001$ nm is formed upon annealing of the film. The small discrepancy between the electron diffraction data and X-Ray data can be due to the different magnitudes of the stresses, arising during crystallization of the free-standing film and the film on the Al_2O_3 substrate.

Table 2. The results of the decoding of the X-ray diffraction patterns at Figure 2.

Diffraction maximum number	*hkl*	*d* (nm)	a_0 (nm)
1	111	0.287	0.497 ± 0.001
2	200	0.249	
3	220	0.176	
4	311	0.150	

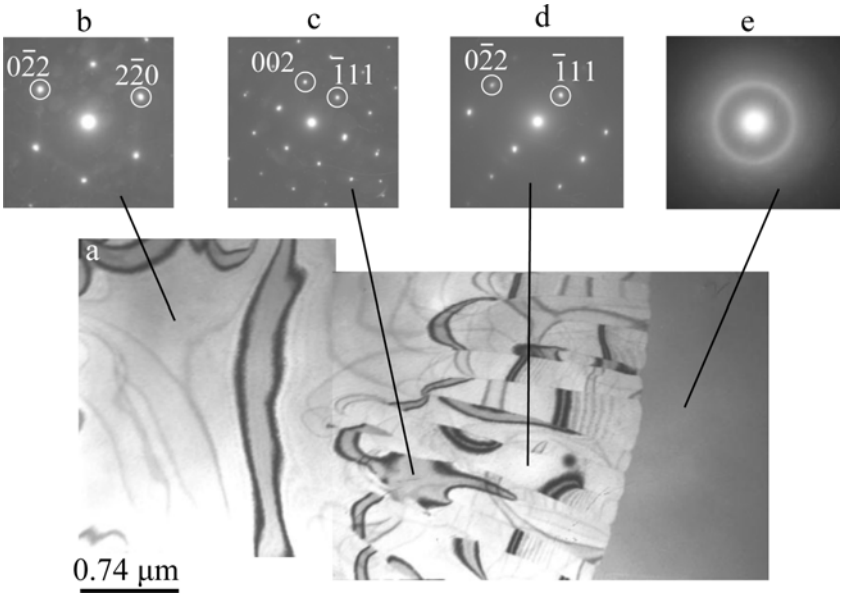

Fig. 3. Crystallization of the amorphous $Ti_{41}Zr_{41}Ni_{18}$ film. "a" – electron microscope image of the partially crystallized film. SAED patterns of different grains, that correspond to the cross sections of the reciprocal lattice "b" – (111), "c" – (110) and "d" – (211). e – SAED patterns of amorphous phase.

The impact of the electron beam on the local area of amorphous film initiated the formation of the flat disk-shape crystal (Figs. 3 and 4). In most cases, at the initial stage of growth, its (111) plane was parallel to the film surface. The (111) section of the reciprocal lattice is represented with the selected area electron diffraction (SAED) pattern in Figure 3b. The action of tensile stresses, caused by different densities of the amorphous and crystalline phases, induced bending and subsequent splitting of the crystal into ribbon blocks of different orientations (Figs. 3c, 3d). This is evidenced by the sharp contrast of the bend contours, which breaks at the grain boundaries.

Figure 4 shows video frames of crystals growth in an amorphous film of $Ti_{41}Zr_{41}Ni_{18}$. Based on the frame-by-frame analysis of this videos, the dependences on time t of the crystal radius $R(t)$ and area $S(t)$ were plotted. The dependence $R(t)$ is shown in Figure 5a. The straight line was plotted by the data of R measurements using the least-squares technique. The correlation coefficient, characterizing the closeness of linear relation between R and t, is close to unity. A linear dependences $R(t)$ takes place:

$$R = 2.732t + 0.028\,\mu\text{m}, \tag{4a}$$

$$R = 0.953t + 0.001\,\mu\text{m}. \tag{4b}$$

Relations (4a) and (4b) correspond to the video frames of crystal 1 and crystal 2, shown in Figures 4a and 4b respectively. According to it the tangential growth rate of the crystal 1 $v_{\tau 1} = 2.732\,\mu\text{m}\cdot\text{s}^{-1}$ and of the crystal 2 $v_{\tau 2} = 0.953\,\mu\text{m}\cdot\text{s}^{-1}$ (these data are listed in Tab. 2). The inequality $v_{\tau 1} > v_{\tau 2}$ indicates that the tangential crystal growth rate increases with increasing of the dose rate of the irradiation, which was $\sim 39.8 \times 10^4\,\text{e}^-/\text{Å}^2\cdot\text{s}$ for the crystal 1 and $\sim 6.4 \times 10^4\,\text{e}^-/\text{Å}^2\cdot\text{s}$ for the crystal 2. The constancy of the growth rate indicates its independence from the electron dose. However, it determined the final size of the crystal.

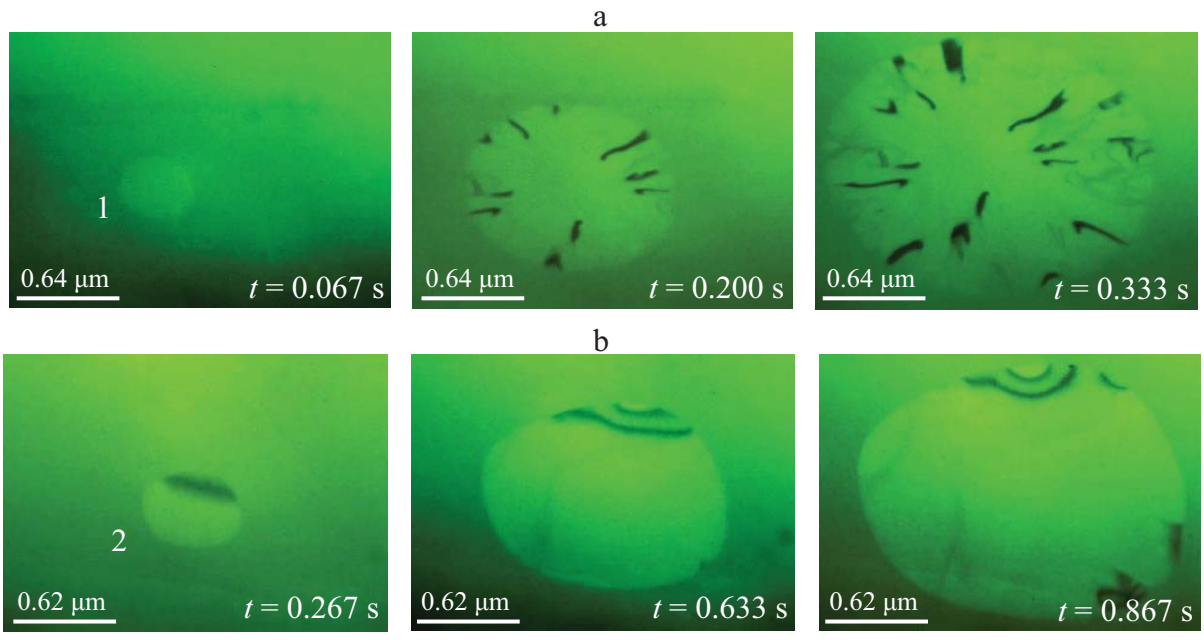

Fig. 4. Video frames of the growth of crystal 1 (a) and crystal 2 (b) in the amorphous film of $Ti_{41}Zr_{41}Ni_{18}$. The time t, elapsed since the start of the video recording, is indicated in the lower right corner of each frame.

According to the relation (4a) during the growth time $t = 0.328$ s, the radius of the crystal 1 increased from 0.028 to 0.896 μm. In this case the electron dose was $\sim 13.1 \times 10^4$ $e^-/Å^2$. According to the relation (4b) during the growth time $t = 0.893$ s, the radius of the crystal 2 increased from 0.001 to 0.851 μm. In this case the electron dose was $\sim 5.7 \times 10^4$ $e^-/Å^2$.

The dependence $S(t)$ is shown in Figure 5b. In the $S - t^2$ coordinates, the experimental data fit well into straight lines. The quadratic dependence $S(t)$ takes place:

$$S = 23.767t^2 + 0.071\ \mu m^2, \tag{5a}$$

$$S = 2.845t^2 + 0.004\ \mu m. \tag{5b}$$

Relations (5a) and (5b) correspond to the video frames of crystal 1 and crystal 2, shown in Figures 4a and 4b respectively.

At the end of filming (at time moment $t_f = 0.328$ s) the area, occupied by the crystal 1 $S(t_f) = 2.637\ \mu m^2$. Similarly for crystal 2 $t_f = 0.893$ s and $S(t_f) = 2.272\ \mu m^2$. Taking into account these data and relation (1), time dependence of the crystalline fraction $x(t)$ was plotted (Fig. 6). The quadratic dependences $x(t)$ takes place:

$$x = 9.012t^2 + 0.027, \tag{6a}$$

$$x = 1.252t^2 + 0.002. \tag{6b}$$

Relations (6a) and (6b) correspond to the video frames of crystal 1 and crystal 2, shown in Figures 4a and 4b respectively.

The passage of electrons through the film causes its Joule-Lenz heating (excitation of phonons) and can creates radiation damage. For excitation of phonons, energy of $\sim$ 0.01 eV is sufficient [13]. Therefore, heating of the film to one degree or another is always present. When using accelerating voltage of 100–125 kV and a current of 50–75 μA without a condenser diaphragm and with appropriate beam focusing at the object, it is possible to obtain a high temperature, sufficient not only for crystallization of amorphous Fe-C films [14], but also for the melting of refractory materials, such as carbon [15]).

An important damage to unstable and organic substances is ionization, which leads to the chemical decomposition of a substance under the influence of an electron beam. Elementary radiation action is the direct knocking out of atoms from their positions and the formation of primary point defects. Their coagulation (at the appropriate temperature) can initiate the crystallization of an amorphous substance, that is resistant to chemical decomposition.

To create radiation damage, an electron must transfer energy to atom E_T, that exceeds the threshold displacement energy E_D (24–40 eV for metals [16]). With an accelerating voltage of 100 kV, the electron energy $E = 100$ keV. The masses of the atoms, that make up the film under study, are $M_{Ti} \sim 7.95 \times 10^{-26}$ kg, $M_{Zr} \sim 1.51 \times 10^{-25}$ kg and $M_{Ni} \sim 9.74 \times 10^{-26}$ kg. According to the relation [16]

$$E_T = 2\,E{\cdot}(E + 2m_0c^2)M^{-1}c^{-2}, \tag{7}$$

where m_0 is the electron rest mass, M is the mass of the atom and c is the speed of light, we get $E_T \approx 5$ eV for the atom of Ti, $E_T \approx 2$ eV for the atom of Zr and $E_T \approx 4$ eV for

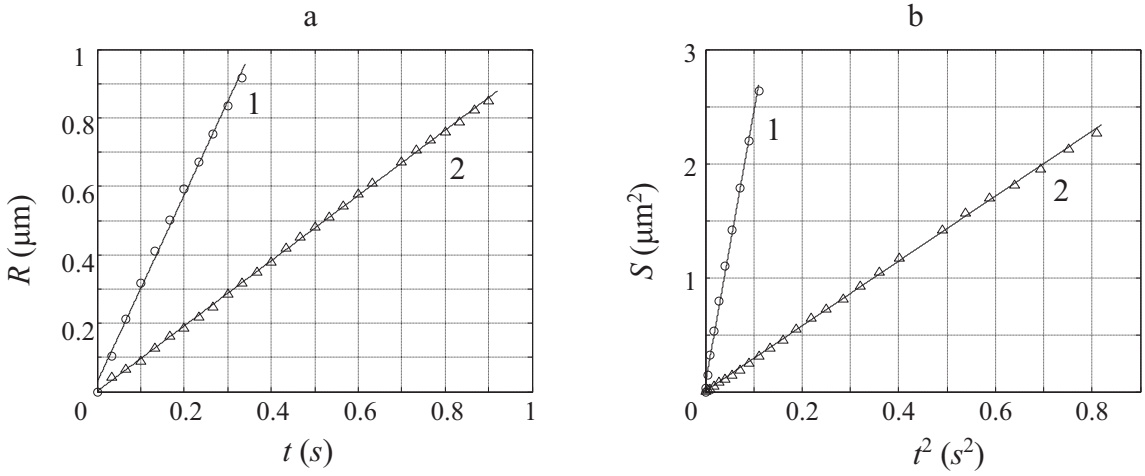

Fig. 5. Kinetic curves of growth of the disk-shaped crystals in amorphous film of $Ti_{41}Zr_{41}Ni_{18}$. (a) Time dependence of the crystals radius R. (b) Time dependence of the crystals area S. Lines 1 and 2 are constructed from the video frames data at Figure 4a (for crystal 1) and Figure 4b (for crystal 2) respectively.

the atom of Ni. This is not enough to create significant radiation damage in the studied film. For example in the case of titanium $E_T \approx 5\,eV \ll E_D \approx 29\,eV$ [16].

Therefore, we are of the opinion, that the main reason for the crystallization of amorphous film in our case is Joule-Lenz heating of the film due to phonon excitation by electrons. This is confirmed by the fact, that in both cases of the electron-beam induced and heat-induced crystallization of $Ti_{41}Zr_{41}Ni_{18}$ film phase transformation has a one-stage character and leads to the formation of crystals with the same fcc lattice (Tabs. 1 and 2).

In addition, previous studies of amorphous films of Cr_2O_3, obtained by laser sputtering of chromium in an oxygen atmosphere, have shown that there are no significant differences between the electron-beam induced and heat-induced crystallization. The impact of an electron beam ($E = 100$ keV) on amorphous free-standing film was initiated growth of a rounded and crescent-shaped Cr_2O_3 crystals with a hexagonal lattice [17]. A similar structure and morphology of Cr_2O_3 crystals was observed during thermal annealing of amorphous free-standing film in a muffle furnace for five minutes at a temperature of 400 °C [18]. There was a strong diffraction contrast of extinction bend contours (depicting the regions where Bragg's law is satisfied), caused by a change in the density of the substance during crystallization. The only difference was in the distribution of crystals over the area of the film. During thermal initiation, crystals grew over the entire area of the film, while during electron beam initiation, they grew only in the region of the electron beam impact. Dominant role of the heat-induced crystallization of amorphous a-GeAu films under the action of an electron beam also was noted in [19].

However, the situation may change with increasing of electrons energy, acting on the film. For example, when $E = 400$ keV, for an atom of Ti according to (7) $E_T \approx 25\,eV \sim E_D \approx 29\,eV$. In this case contribution of the electron-beam induced crystallization can increase significantly. The differences between the electron-beam induced and heat-induced crystallization of amorphous films of $Ge_2Sb_2Te_5$ with electrons with $E = 200$ and 400 keV were previously described in [20].

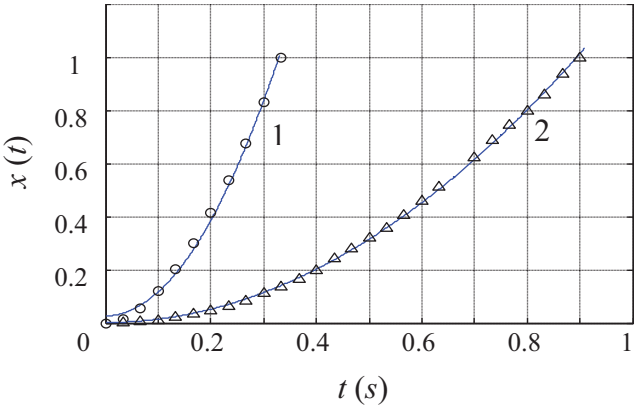

Fig. 6. Time dependence of the crystalline fraction $x(t)$ in the film. Lines 1 and 2 are constructed from the video frames data at Figure 4a (for crystal 1) and Figure 4b (for crystal 2) respectively.

4 Conclusions

X-ray amorphous state of the $Ti_{41}Zr_{41}Ni_{18}$ coating is preserved up to a temperature of 650 °C. At a temperature of 700 °C, the coating crystallizes. Irradiation of amorphous film of $Ti_{41}Zr_{41}Ni_{18}$ with the electron beam initiates its crystallization. The transformation has one-stage character. The amorphous medium polymorphically passes into the crystalline one with fcc structure. According to the video recording data (Figs. 4a, 4b) during crystallization of the film a single disc-shaped crystal grows in the field of observation. The crystal grows at the constant rate at the

Table 3. Kinetic characteristics of crystal growth in an amorphous film of $Ti_{41}Zr_{41}Ni_{18}$.

An object	Tangential growth rate v_τ	Characteristic unit of time t_0	Characteristic unit of length D_0	Relative length δ_0
Crystal 1	$2.732\,\mu m \cdot s^{-1}$	0.259 s	1.471 μm	2930
Crystal 2	$0.953\,\mu m \cdot s^{-1}$	0.709 s	1.353 μm	2700

constant intensity of electron beam irradiation of the film. In this case the radius of the crystal $R \sim t$, the area of the crystal $S \sim t^2$ and the crystalline fraction $x \sim t^2$.

The observed features of crystal growth allow us to make the qualitative conclusion, that layer polymorphous crystallization (LPC) of amorphous film takes place [21,22]. The quantitative feature of LPC is the value of the relative length δ_0 [23], determined as

$$\delta_0 = \frac{D_0}{a_0}, \tag{8}$$

where a_0 is the lattice parameter of the crystal. D_0 is the characteristic unit of length. According to [24] D_0 is the average crystal size at the time $t = t_0$. t_0 is the characteristic unit of time, after which the volume of the amorphous phase decreases by the factor of $e = 2.718$. At this moment the fraction of the crystalline phase $x = x_0 = 0.632$. The dimensionless parameter δ_0 is the number of elementary cells of the crystal, which fit at the distance, equal to D_0.

Substituting x_0 into (6a) and (6b), we obtain the numerical values of t_0. For crystals 1 and 2 (Figs. 4a, 4b) $t_{01} = 0.259$ s and $t_{02} = 0.709$ s respectively. Substituting t_0 into (4a) and (4b) and multiplying by 2, we obtain the numerical values of D_0. For crystals 1 and 2 $D_{01} = 1.471$ μm and $D_{02} = 1.353$ μm respectively. Substituting D_0 into (8), we obtain the numerical values of the relative length δ_0. For crystals 1 and 2 $\delta_{01} \approx 2930$ and $\delta_{02} \approx 2700$ respectively. The obtained values of t_0, D_0 and δ_0 are shown in Table 3.

Currently available data, concerning the electron-beam crystallization of amorphous films, are classified by structural and morphological characteristics (qualitatively) and by the numerical value of the relative length δ_0 (quantitatively) [25]. Wherein layer polymorphous crystallization mode, describes the nucleation and growth of a single-crystal layer in the field of the electron-beam impact. For it δ_0 is about several thousand. Time dependence $x(t)$ is quadratic. Island polymorphous crystallization mode, describes the nucleation and growth of the polycrystalline layer, for which δ_0 is about several hundred. Time dependence $x(t)$ is exponential. Dendrite polymorphous crystallization mode describes the nucleation and growth of dendrite, for which δ_0 is about several thousand. Time dependence $x(t)$ is quadratic.

The structural and morphological characteristics, given in this work and the numerical value of the relative length δ_0 correspond to the layered polymorphous crystallization mode of the amorphous film of $Ti_{41}Zr_{41}Ni_{18}$.

The authors are grateful to the engineer Nikolai Reznik for technical assistance in conducting of the electron microscopic studies and to Maria Sokol for assistance in the design of the article.

Author contribution statement

Aleksandr Bagmut: statement of the research problem and TEM investigation. Ivan Bagmut: computer analysis and processing of TEM results. Aleksandr Devizenko: magnetron deposition and X-ray investigation. All the authors were involved in the preparation of the manuscript. All the authors have read and approved the final manuscript.

References

1. K.F. Kelton, W.J. Kim, R.M. Stroud, Appl. Phys. Lett. **70**, 3230 (1997)
2. A.M. Viano, E.H. Majzoub, R.M. Stroud, M.J. Kramer, S.T. Misture, P.C. Gibbons, K.F. Kelton, Philos. Mag. A **78**, 132 (1998)
3. V. Brien, A. Dauscher, P. Weisbecker, F. Machizaud, Appl. Phys. A **76**, 187 (2003)
4. V. Brien, A. Dauscher, P. Weisbecker, J. Ghanbaja, F. Machizau, J. Cryst. Growth **256**, 407 (2003)
5. V. Azhazha, S. Dub, G. Khadzhay, B. Merisov, S. Malykhiny, A. Pugachov, Philos. Mag. **84**, 983 (2004)
6. S.V. Malykhin, V.V. Kondratenko, I.A. Kopylets, S.V. Surovitskiy, I.G. Shipkova, I.F. Mikhailov, E.N. Zubarev, Yu.S. Bogdanov, J. Nano-Electron. Phys. **11**, 04011 (2020)
7. S.V. Malykhin, V.V. Kondratenko, I.A. Kopylets, S.V. Surovitskiy, A.A. Baturin, I.F. Mikhailov, M.V. Reshetnyak, S.S. Borisova, Yu.S. Bogdanov, J. Nano-Electron. Phys. **11**, 03009 (2019)
8. V. Brien, A. Dauscher, S. Weber, J.B. Ledeuil, F. Machizaud, Bulg. J. Phys. **29**, 142 (2002)
9. H. Huang, D. Meng, X. Lai, Y. Zhao, P. Zhou, Q. Wang, H. Huang, J. Qiang, Vacuum **122**, 147 (2015)
10. I.F. Mikhailov, A.A. Baturin, A.I. Mikhailov, S.S. Borisova, Funct. Mater. **18**, 150 (2011)
11. A.G. Bagmut, I.A. Bagmut, J. Non-Cryst. Solids **547**, 187 (2020)
12. A.L. Patterson, Phys. Rev. **56**, 978 (1939)
13. L.W. Hobbs, Radiation effects in analysis of inorganic specimens by TEM, in: Introduction to Analytical Electron Microscopy, edited by J.J. Hren, J. I. Goldstein, D. C. Joy (Plenum, New York, 1979), pp. 437–490

14. S.M. Zharkov, L.I. Kveglis, Phys. Solid State **46**, 969 (2004)
15. H. König, Naturwissenschaften **34**, 108 (1947)
16. M.W. Thompson, Defects and Radiation Damage in Metals (Cambridge University Press, London, 1969)
17. A.G. Bagmut, V.A. Zhuchkov, D.V. Melnichenko, Funct. Mater. **14**, 351 (2007)
18. V. Yu. Kolosov, K.L. Shvamm, A.G. Bagmut, S.N. Grigorov, J. Surface Invest. **10**, 100 (2004)
19. L. Ba, Y. Qin, J. Appl. Phys. **80**, 6170 (1996)
20. B.J. Kooi, W.M.G. Groot, J.Th.M. De Hosson, J. Appl. Phys. **95**, 924 (2004)
21. U. Köster, U. Herold, in Glassy Metals I. Ionic Structure, Electronic Transport, and Crystallization, edited by H.-J. Güntherodt, H. Beck. (Springer, Berlin Heidelberg, New York, 1981)
22. A.G. Bagmut, Tech. Phys. Lett. **38**, 488 (2012)
23. A.G. Bagmut, Funct. Mater. **26**, 6 (2019)
24. A.N. Kolmogorov, Izv. Acad. Sci. USSR, Ser. Math. **1**, 355 (1937)
25. A.G. Bagmut, Probl. Atom. Sci. Technol. **137**, 64 (2022)

Cite this article as: Aleksandr Bagmut, Ivan Bagmut, and Aleksandr Devizenko, In situ TEM study of crystals growth in amorphous Ti-Zr-Ni films at electron beam irradiation, Eur. Phys. J. Appl. Phys. **98**, 34 (2023)